Boosting the Interfacial Dynamics and Thermodynamics in Polyanion Cathode by Carbon Dots for Ultrafast-Charging Sodium Ion Batteries

Yujin Li [a], Yu Mei [a], Roya Momen [b], Bai Song [c], Yujie Huang [a], Xue Zhong [a], Hanrui Ding [a], Wentao Deng [a], Guoqiang Zou [a], Hongshuai Hou [a,*] and Xiaobo Ji [a]

[a] State Key Laboratory of Powder Metallurgy, College of Chemistry and Chemical Engineering, Central South University, Changsha, 410083, China
E-mail: hs-hou@csu.edu.cn

[b] Department of Chemistry and Shenzhen Grubbs Institute, Southern University of Science and Technology, Shenzhen 518055 (China)

[c] Dongying Cospowers Technology Limited Company, China

1. Experimental section

1.1 Materials synthesis

N/S co-doped carbon dots were prepared through our previous reported method.[1] Pure $Na_3V_2(PO_4)_3$, N/S co-doped carbon coated $Na_3V_2(PO_4)_3$ composites, referred to as NVP and NVP/NSC, respectively, were synthesized by a one-step solid phase ball milling followed by sintering method. The N/S co-doped carbon dots were used as the reducing agent, carbon source, nitrogen source and sulfur source simultaneously. In a typical NVP/NSC synthesis method, 2 mmol V_2O_5, 6 mmol $NH_4H_2PO_4$, 3 mmol Na_2CO_3 and 50/75/100 mg N/S doped carbon dots were ball milled in an agate ball mill jar at 500 rpm for 6 h, where the bead ratio is approximately 15:1. The chemicals above were purchased from Aladdin (Shanghai, China). The resulting precursors were then placed in a tube furnace at 350°C for 4 h under an argon gas (Ar) atmosphere and then heating up to 850 °C at a rate of 5 °C/min. The intermediate powder was remelted and sintered for 8 h at 850 °C. The synthesis process for bare NVP was the same as the preparation of NVP/NSC, but without the addition of N/S co-doped carbon dots.

1.2 Materials characterization

Determination of elemental content (C, N and S) was carried out with the elemental analyzer (EA, Elementar Vario EL Cube, GER). The samples were characterized by Fourier transform infrared spectroscopy (FT-IR, AVTA-TAR, 370) to detect characteristic functional groups. The crystal structures were characterized by X-ray diffractometer (XRD Rigaku D/max-2550 VB + 18 KW, Cu Kα radiation, Japan). The data were then analysed using the Rietveld structure refinement program on FullProf. Raman spectra were obtained with a RENISHAW invia wire 4.2 spectrometer. Elemental composition and valence states were determined by X-ray photoelectron spectroscopy (XPS, Thermo Scientific K-Alpha, USA). Microscopic morphology of samples was observed by scanning electron microscopy (SEM, JEOL/JSM-7610FPlus). Detailed microstructures were observed by using a transmission electron microscope (TEM, FEI Titan G2 60-300, USA), and TEM-energy-dispersive spectroscopy (EDS) analysis was carried out by using a Bruker Super EDS detector.

1.3 Electrochemical measurements

The button cells (CR 2016) were assembled in an argon-filled glove box with water and oxygen content below 0.5 ppm. A 70 wt% NVP-based sample was mixed with carbon black (Super P) (20 wt%) and polyvinylidene fluoride (PVDF) (10 wt%) in N-methylpyrrolidone (NMP) solvent to form uniform slurry and then pasted it onto a carbon coated aluminum foil, followed by vacuum drying oven at 120 °C for 12 h to prepare the positive electrode. The mass loading was 0.8 ~ 1.0 mg cm^{-2}. Sodium metal was used as the reference and counter electrode,

$NaClO_4$ in propylene carbonate (PC) and 5% fluoroethylene carbonate (FEC) (1.0 mol/L) was utilized as the electrolyte and Whatman GF/D was employed as the separator. These half-cells were subjected to constant current charge/discharge testing on a LAND CT2001 testing system (Wuhan LAND Electronics. Ltd., China) with a voltage range of 2.3-4.0 V (vs. Na^+/Na). Electrochemical impedance spectra (frequency range: 0.01-10^5 Hz) and cyclic voltammetry (CV) were using Chenhua electrochemical workstation (CHI 660D, Chenhua, Shanghai) and Autolab electrochemical workstation (MULTI AUTOLAB M204). For the galvanostatic intermittent titration technique (GITT), a constant current of 0.1 C (1 C= 117 mA g^{-1}) was applied for 20 min and then interrupted to achieve an open circuit condition for 120 min. The procedure was repeated until the electrode potential reached the cut-off voltage. In addition, a sodium ion full cell was constructed using NVP/NSC-75 as the cathode and hard carbon (HC) as the anode. The HC (Kuraray Co., Ltd, 70 wt%) was mixed with carbon black (20 wt%) and carboxymethyl cellulose (10 wt%) in H_2O solvent to form unique slurry, and then pasted onto a copper foil, followed by vacuum drying oven at 100 °C for 12 h to prepare the negative electrode. The HC anode was cycled between a voltage range of 0.01-2.0 V (vs. Na^+ /Na) at a current of 0.5 A g^{-1} for 8 cycles to reach a steady state before the full cell was assembled. The full cell has a cathode to anode capacity ratio of approximately 1:1.2 and the cell capacity is determined by the cathode. Charge and discharge measurements were carried out between 1.2 V and 3.6 V at 5 C (1 C = 117 mA g^{-1}). For both pre-sodiation and full cells test, 1.0 M $NaPF_6$ in Diglyme was used as electrolyte.

1.4 Theoretical calculations

Structural optimization was performed by Vienna Ab-initio Simulation Package (VASP) [2]with the projector augmented wave (PAW) method.[3] In order to describe the weak interactions between atoms, the exchange-functional was treated using the Perdew-Burke-Ernzerhof (PBE)[4]functional in combination with the DFT-D3 correction.[5] The cut-off energy of the plane-wave basis was set at 450 eV in structural optimization. The Brillouin zone integration was performed with a Monkhorst-Pack *k*-point mesh of 0.04 $Å^{-1}$ to optimise geometry and lattice size. Partial occupancies of the Kohn−Sham orbitals were allowed using the Gaussian smearing method and a width of 0.05 eV. A geometry optimization was considered convergent when the energy change was smaller than 0.05 eV $Å^{-1}$. To consider the strong correlation effects of transition metal in structure, both structural optimizations and electronic structure calculations were carried out by using the spin-dependent GGA plus Hubbard correction U method.

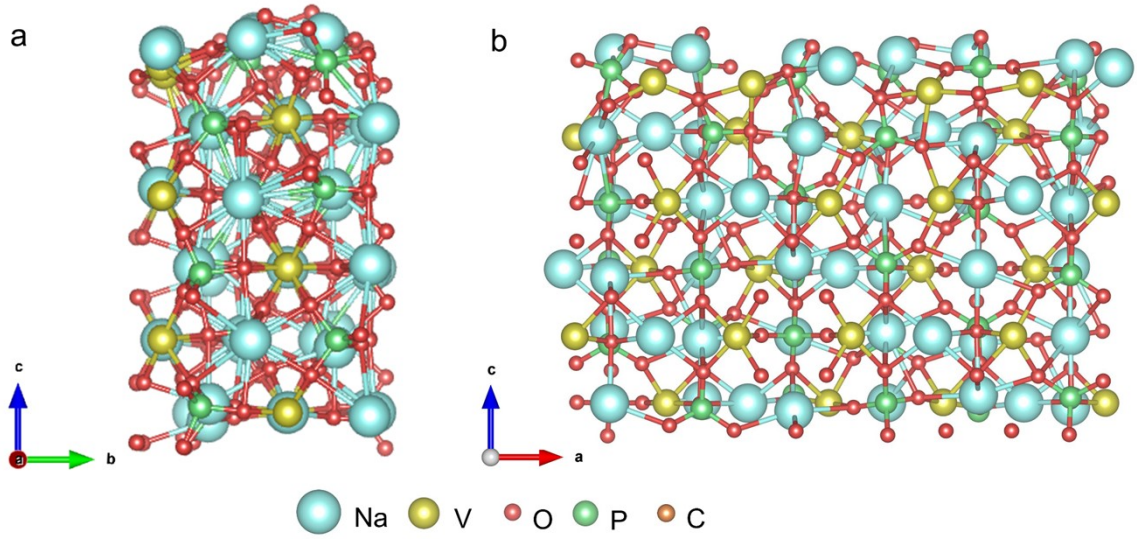

Figure S1. The optimized structure model of the NVP.

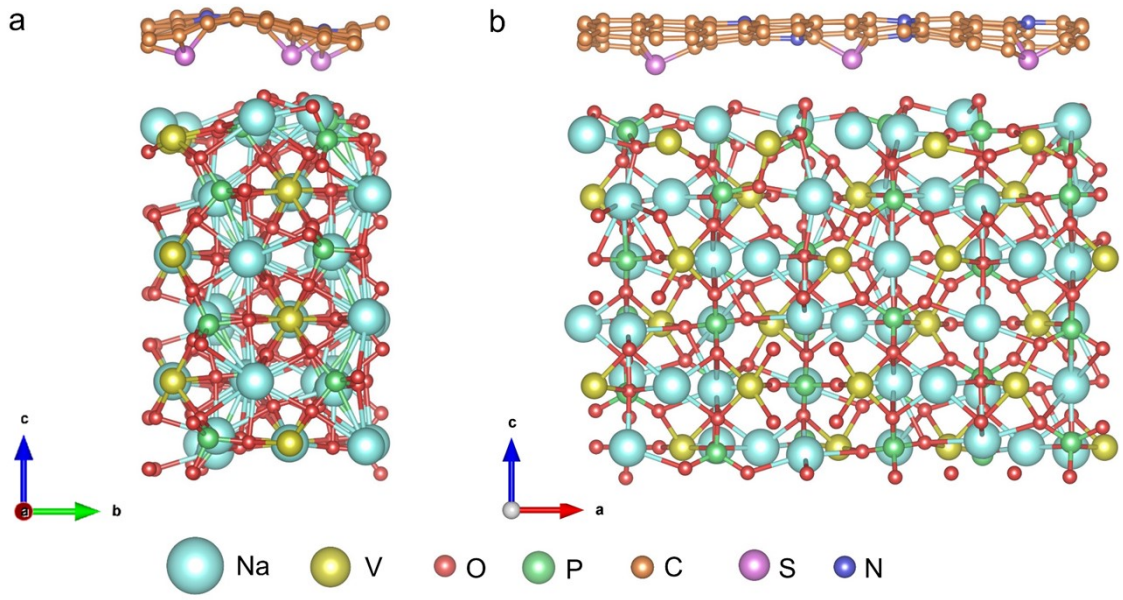

Figure S2. The optimized structure model of the NVP/NSC.

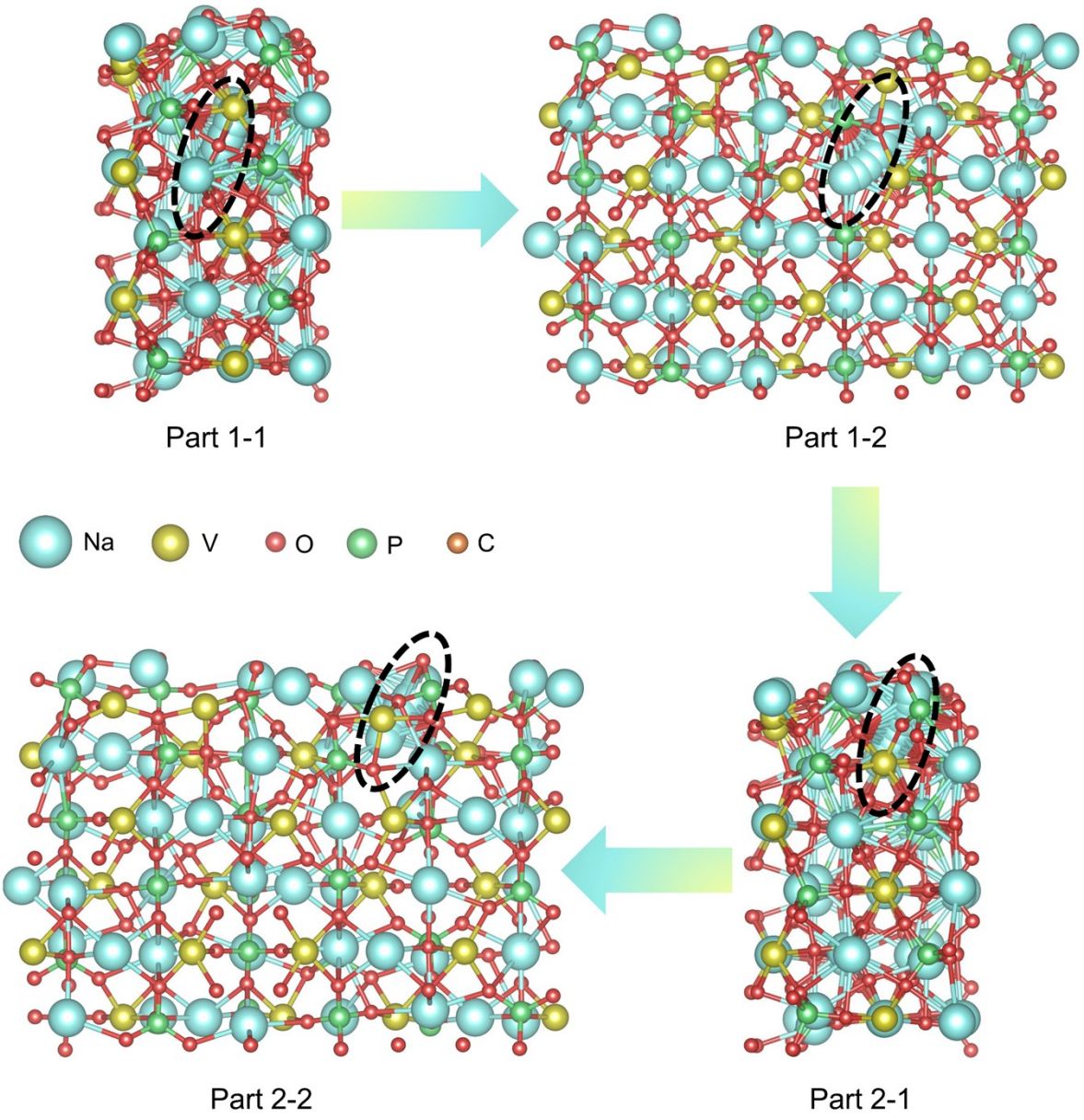

Figure S3. Schematic diagram of Na^+ diffusion pathways and processes alongside Path II[6] in NVP (Inside the dashed box is the migrating sodium ions).

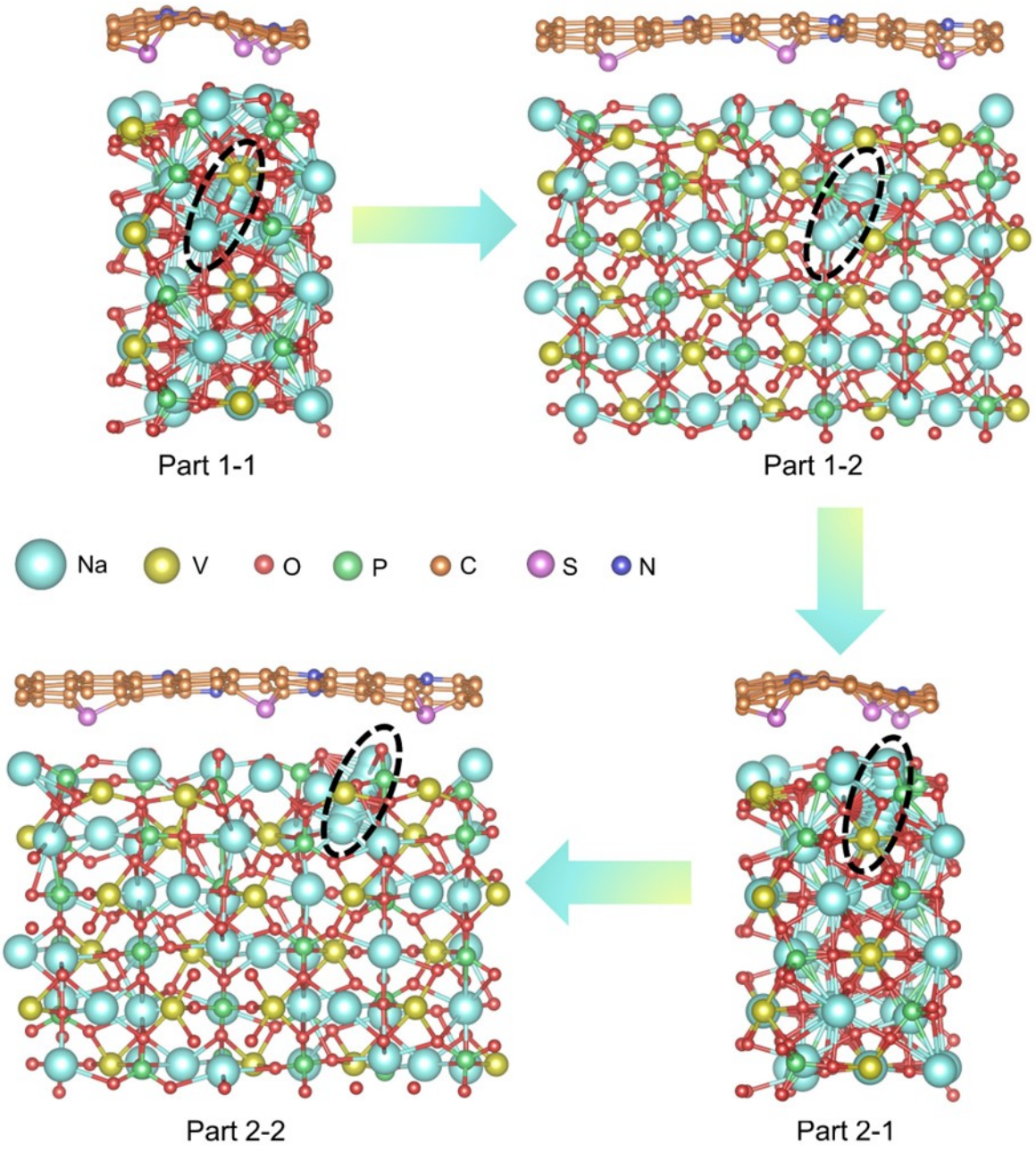

Figure S4. Schematic diagram of Na^+ diffusion pathways and processes alongside Path II[6] in NVP/NSC (Inside the dashed box is the migrating sodium ions).

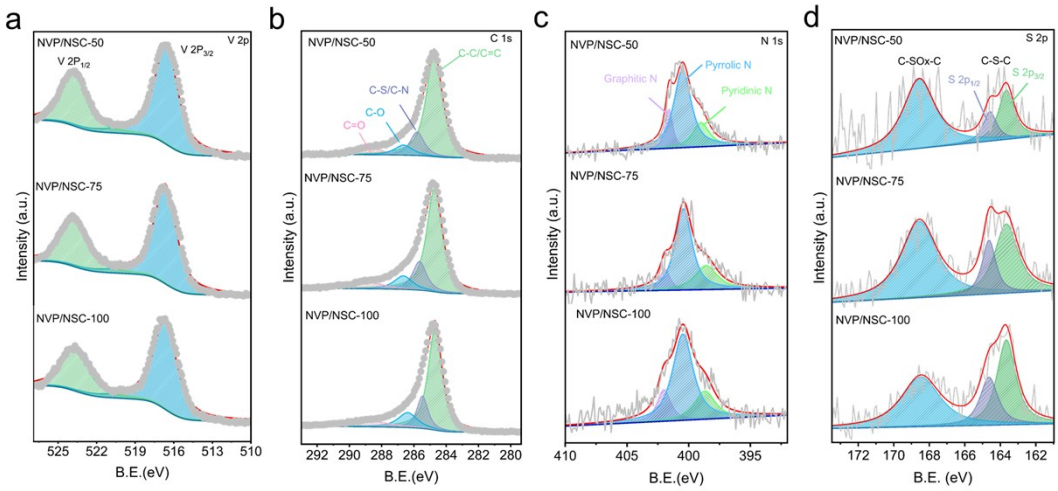

Figure S5. High-resolution XPS spectra of V2p (a), C1s (b), N1s (c) and S2p (d) for the NVP/NSC samples.

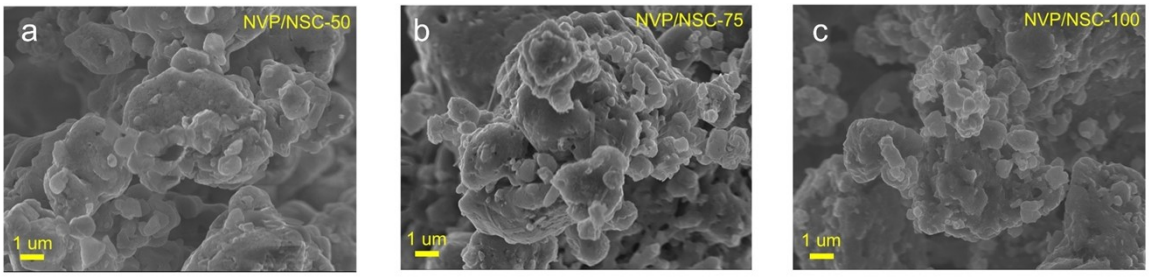

Figure S6. SEM images of NVP/NSC-50 (a), NVP/NSC-75 (b) and NVP/NSC-100 (c).

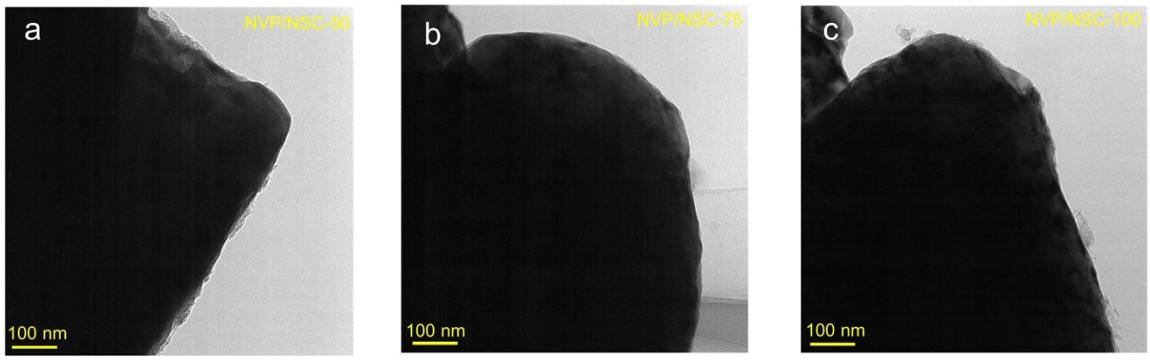

Figure S7. TEM images of NVP/NSC-50 (a), NVP/NSC-75 (b) and NVP/NSC-100 (c).

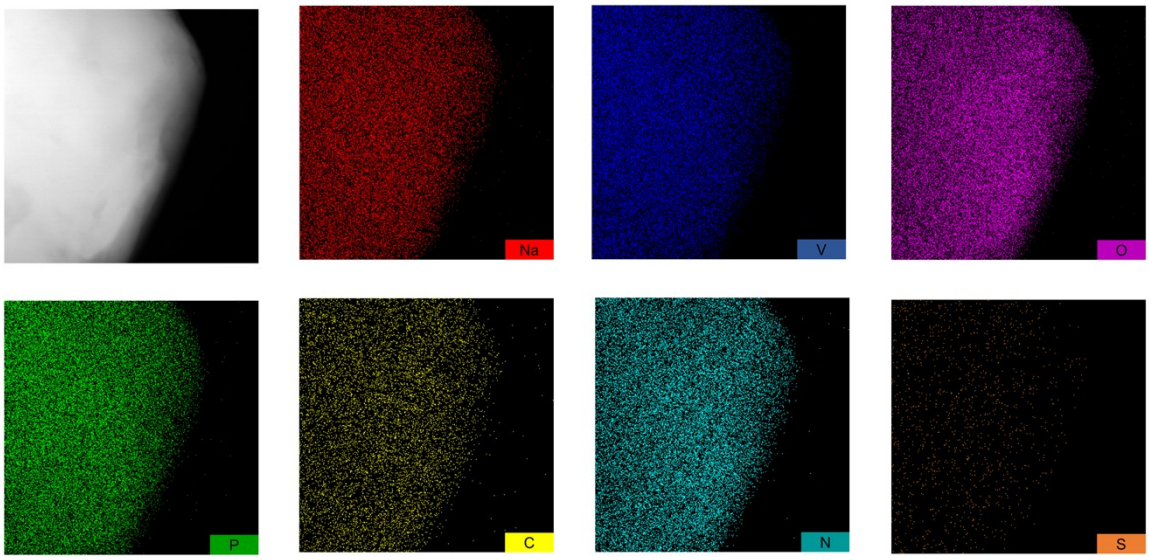

Figure S8. Elemental mapping images for Na, V, O, P, C, N and S in NVP/NSC-50.

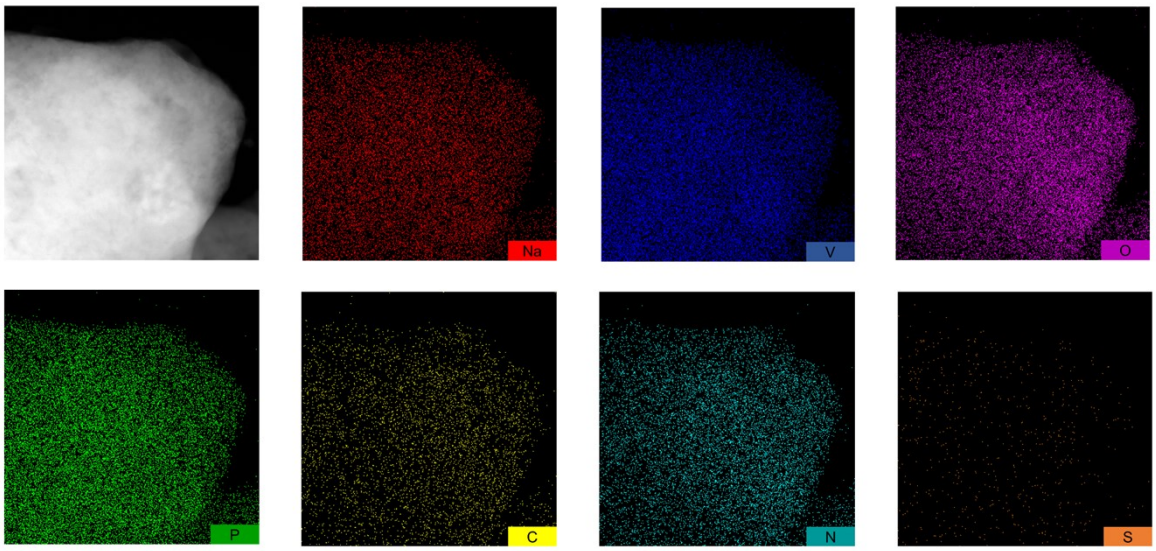

Figure S9. Elemental mapping images for Na, V, O, P, C, N and S in NVP/NSC-100.

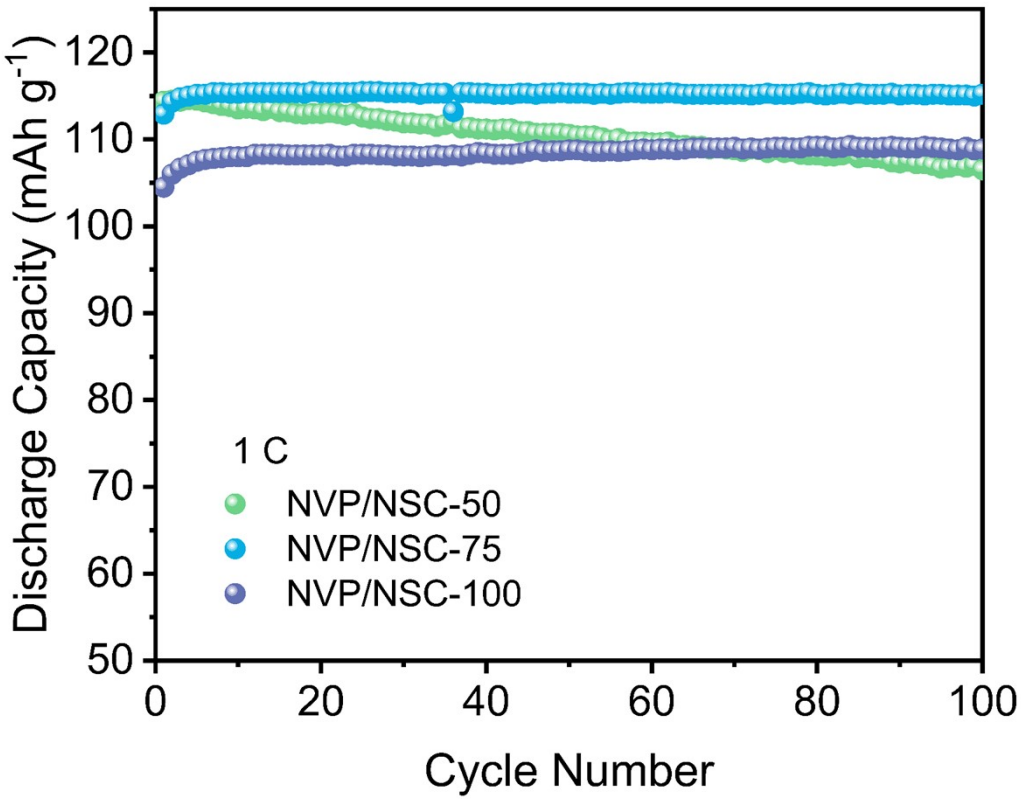

Figure S10. Cycling performances of NVP/NSC samples at the rate of 1 C for 100 cycles.

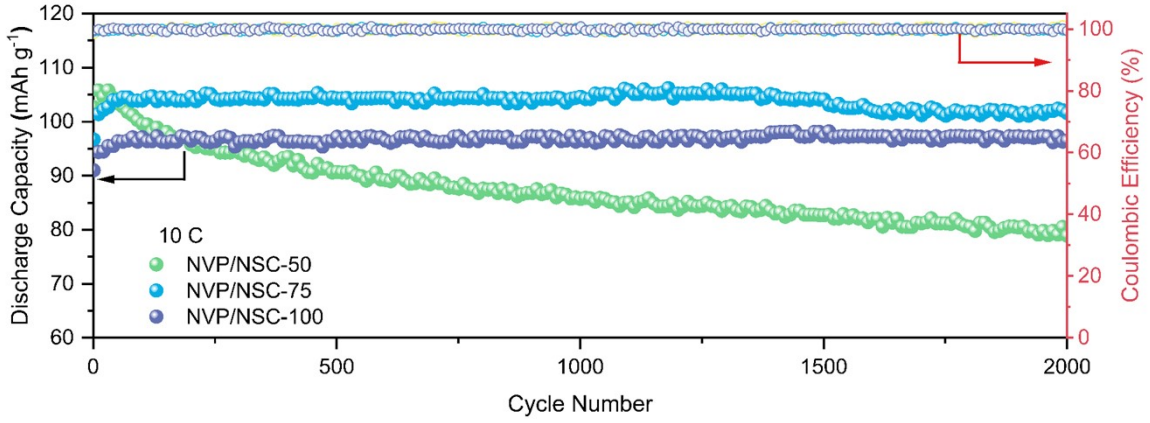

Figure S11. Specific capacities and coulombic efficiencies of NVP/NSC samples at the rate of 10 C for 2000 cycles.

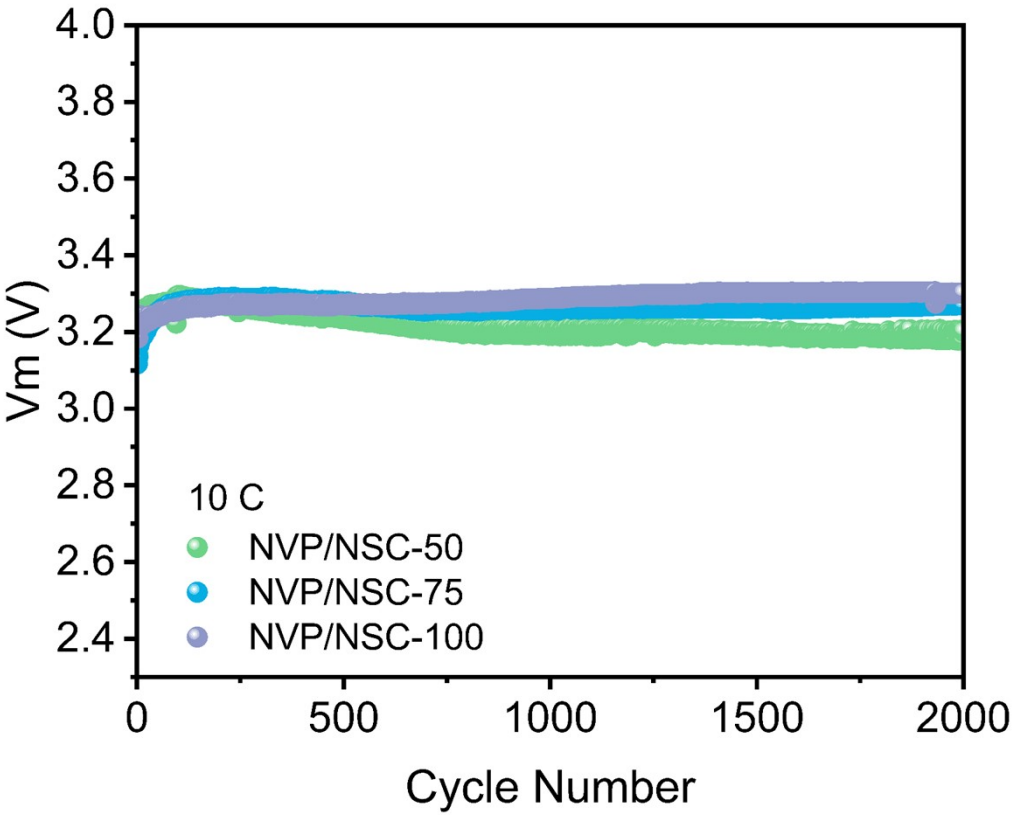

Figure S12. Medium voltages of NVP/NSC samples at the rate of 10 C for 2000 cycles.

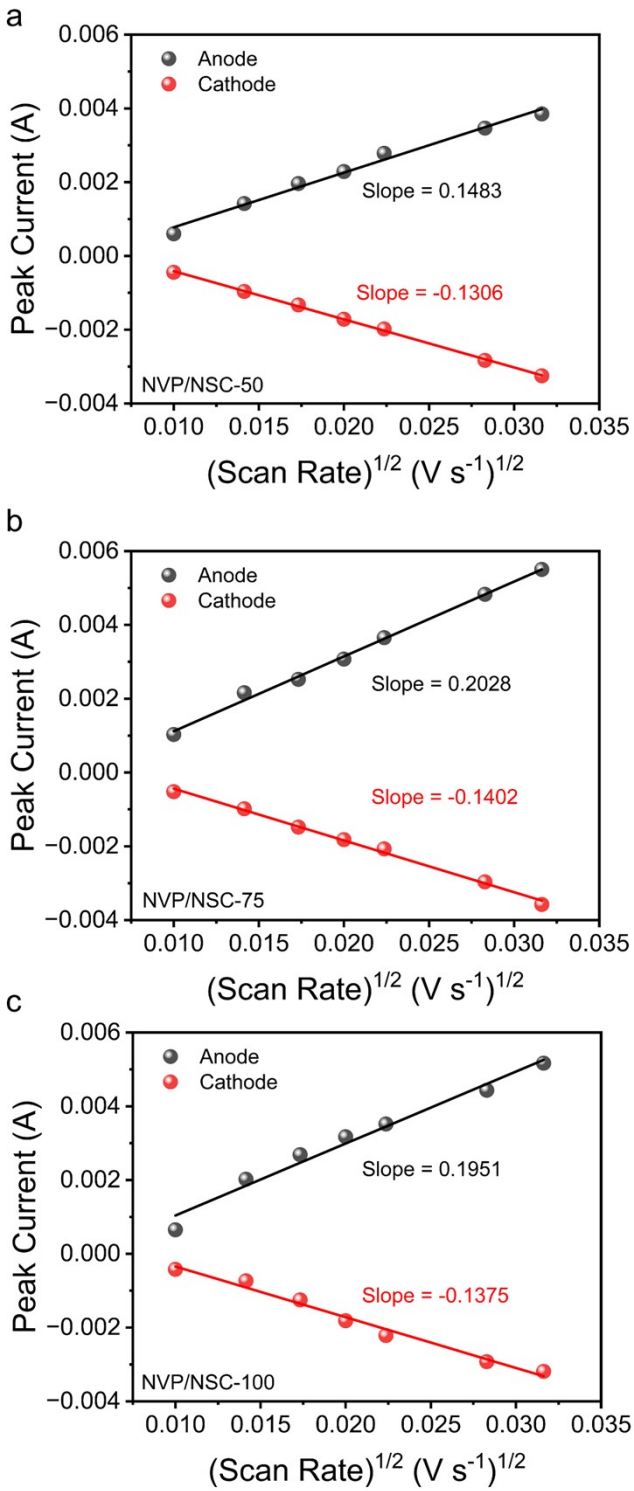

Figure S13. Linear fits for the anodic and cathodic peak currents versus scan rates of (a) NVP/NSC-50, (b) NVP/NSC-75 and (c) NVP/NSC-100.

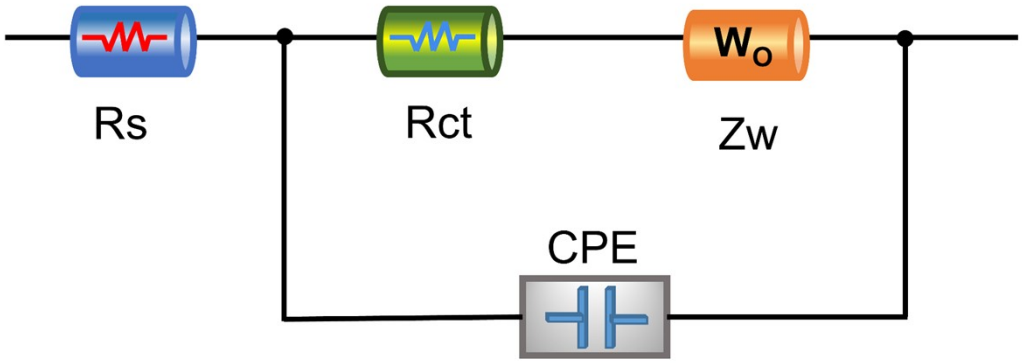

Figure S14. Equivalent circuit model used to fit experimental EIS data.

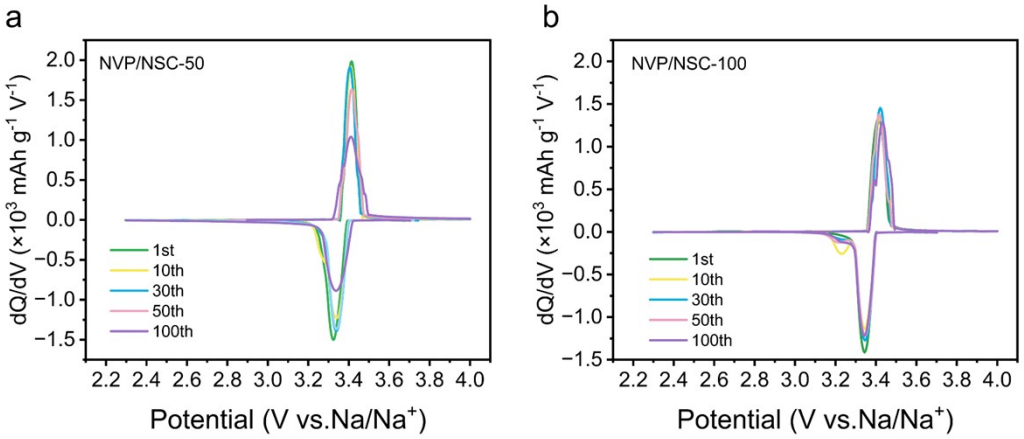

Figure S15. The dQ/dV curves of NVP/NSC-50 (a) and NVP/NSC100 (b) for the selected cycles at 1 C.

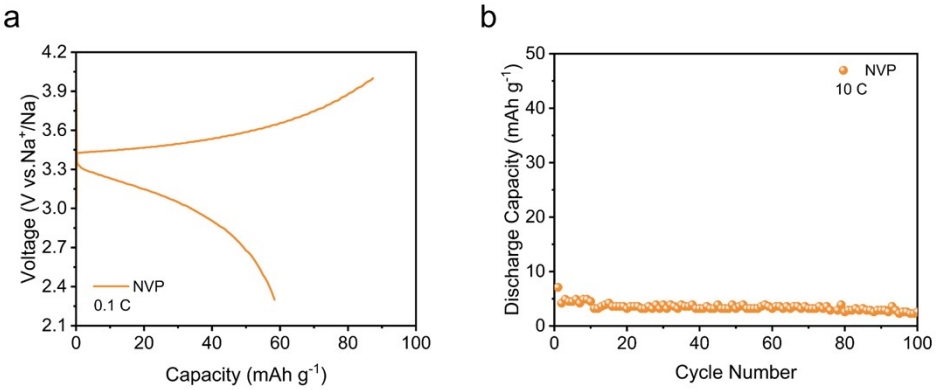

Figure S16. The GCD curves of NVP at 0.1 C (a) and cycling performance at the rate of 10 C after 100 cycles (b).

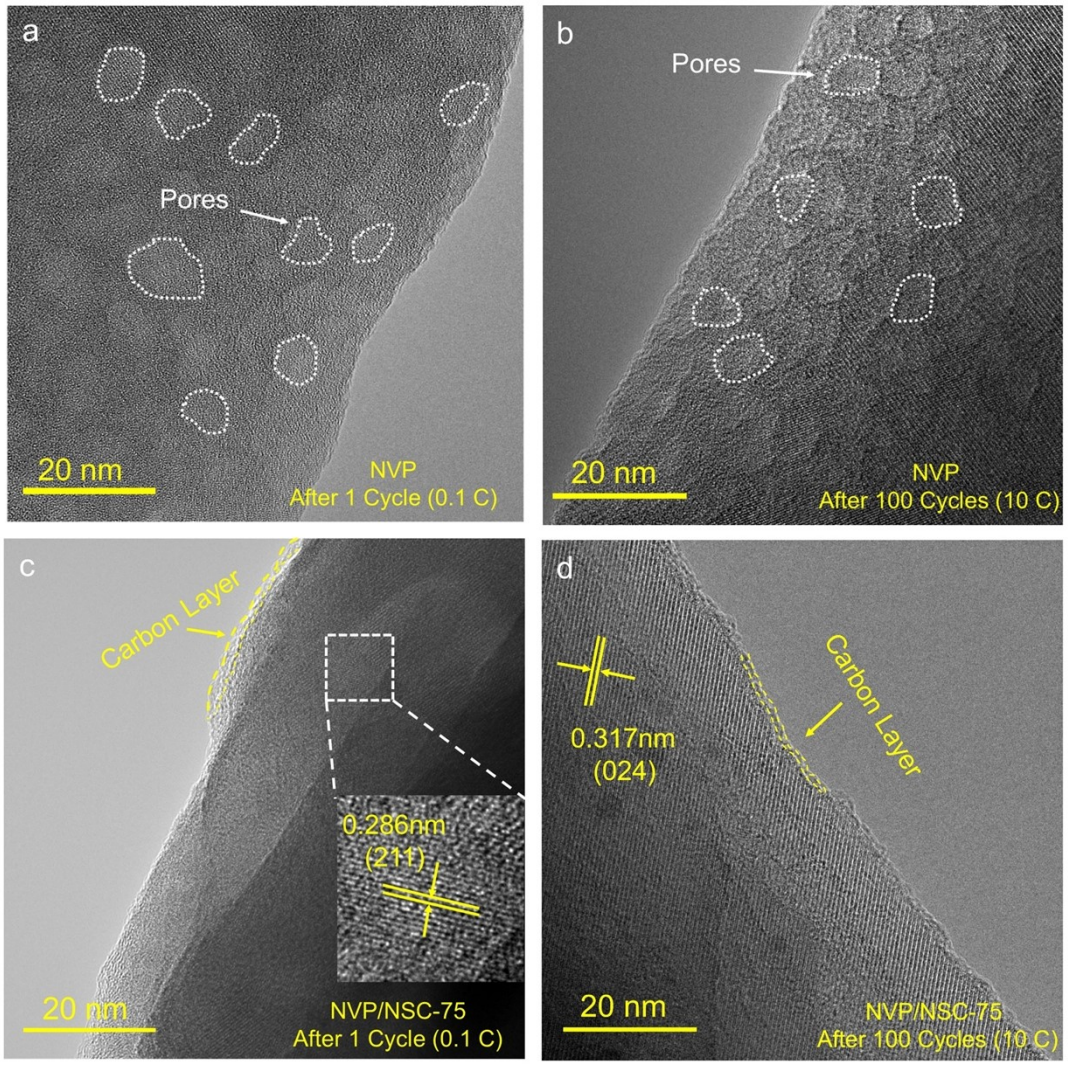

Figure S17. HRTEM images of NVP and NVP/NSC-75 after one cycle at 0.1 C (a, c) and after 100 cycles at 10 C (b, d).

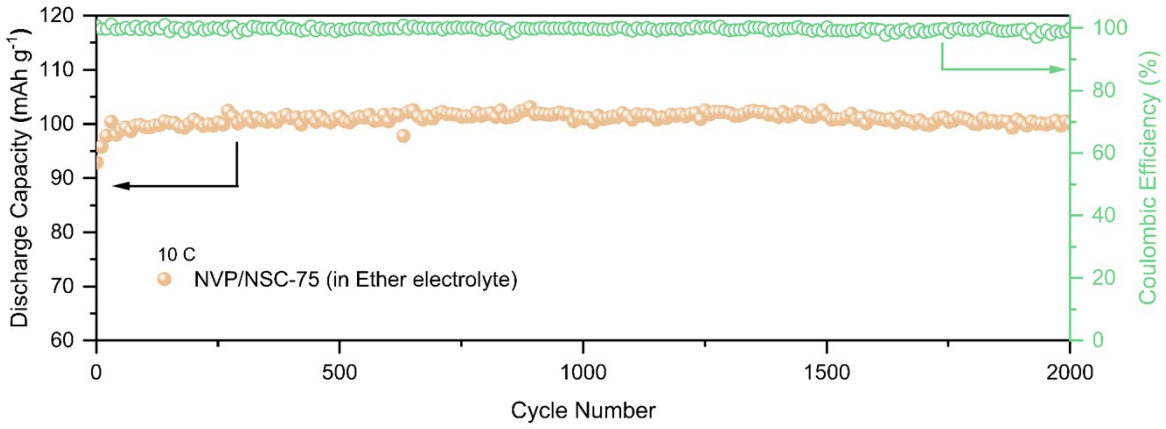

Figure S18. Specific capacity and coulombic efficiency of NVP/NSC-75 at a rate of 10 C for 2000 cycles in ether electrolyte.

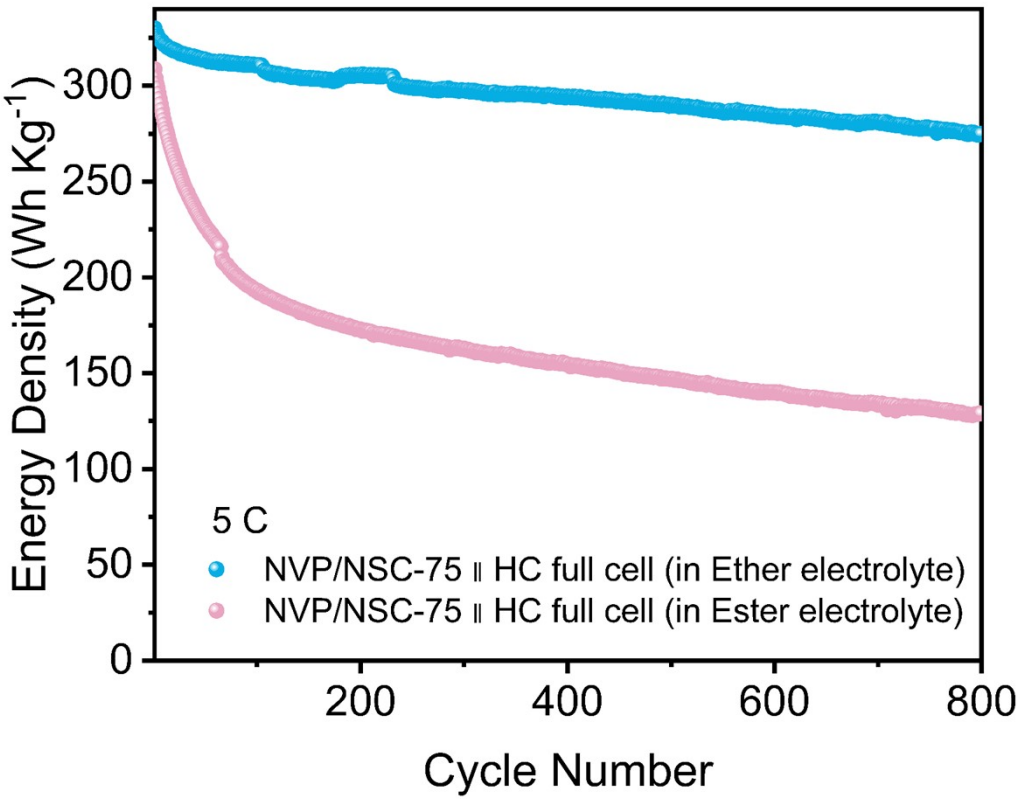

Figure S19. Energy density of NVP/NSC-75 ‖ HC full cell for 800 cycles at 5 C in different electrolyte.

Table S1. Result of structural analysis obtained from XRD Rietveld refinement of samples NVP/NSC-50, NVP/NSC-75 and NVP/NSC-100

Samples	Lattice constant			Reliability factors [%]	
	a (= b) [Å]	c [Å]	V [Å^3]	R_{WP}	R_P
NVP/NSC-50	8.73072 (0.00033)	21.82444(0.00102)	1440.701(0.103)	5.20	3.90
NVP/NSC-75	8.73285 (0.00044)	21.82199 (0.00134)	1441.243(0.136)	7.20	5.34
NVP/NSC-100	8.73197 (0.00043)	21.84524(0.00131)	1442.488(0.132)	4.61	3.51

Table S2. Content ratio of C, N and S in N/S CDs and NVP/NSC series

Samples	C [%]	N [%]	S [%]
N/S CDs	57.13	1.71	4.152
NVP/NSC-50	1.10	0.24	0.099
NVP/NSC-75	2.23	0.45	0.149
NVP/NSC-100	3.43	0.43	0.161

Table S3. Comparison of electrochemical properties of other NVP materials

Material	Carbon content [%]	Voltage window [V]	Rate performance [mAh g^{-1}]	Capacity retention [%]	Ref
NVP/NSC-75	**2.23**	**2.3-4.0**	**83.2 at 100 C 91 at 50 C 98.8 at 20 C**	**72.2 at 10000 cycles at 100 C 86.7 at 10000 cycles at 20 C 97.8 at 2000 cycles at 10 C**	**This work**
$Na_3V_2(PO_4)_3$/C	17.68	2.5-4.0	96 at 20 C	78 at 7000 cycles at 20 C	7
NVP@C-N150	14.50	2.7-3.8	71 at 100 C	91 at 5000 cycles at 20 C	8
HP-NVP@SC	6.48	2.3-3.9	95 at 30 C	91 at 2500 cycles at 20 C	9
NVP@3D-NSC	13.27	2.3-3.9	54 at 80 C	77.6 at 6000 cycles at 20 C	10
NVP@C+N@CNTs	12.68	2.5-4.0	70 at 80 C	87 at 300 cycles at 30 C	11
(C@NVP)@pC	20	2.3-3.9	74 at 100 C	-	12
NVP@rGO	-	2.0-4.0	44 at 50 C	81 at 3000 cycles at 5 C	13
NVP–CNF-6 h	8.34	2.7-4.0	88.9 at 50 C	93 at 300 cycles at 1 C	14
HP-NVP	4.4	2.3-3.9	61 at 100 C	85 at 10000 cycles at 20 C	15
NVP-Ti0.15/ C	-	2.3-3.9	81.6 at 20 C	86 at 500 cycles at 10 C	16
900-NVP@C/G	17.9	2.5-4.0	76 at 60 C	95 at 1000 cycles at 10 C	17
PL-NVP@C	4.95	2.3-3.9	72 at 50 C	91.3 at 2000 cycles at 10 C	18
HCF-NVP	6.41	2.0-3.9	78 at 100 C	54 at 20000 cycles at 30 C	19
NVP/C	2.0	2.0-4.0	70 at 100 C	50 at 5000 cycles at 50 C	20
NVP@C-CNW	2.33	2.3-3.9	62.2 at 60 C	80.6 at 1000 cycles at 20 C	21
NVP@C@HC	16.49	2.0-4.0	60.4 at 50 C	70.7 at 10000 cycles at 20 C	22
NVP-Freestanding	35.1	2.5-4.0	63 at 30 C	88.6 at 150 cycles at 0.5 C	23
NVP/G	6.14	2.2-4.0	70.1 at 30 C	86 at 300 cycles at 5 C	24
NVP/C with 3D porous structure	-	2.0-4.0	74.4 at 50 C	90.4 At 2200 cycles at 20 C	25
NVP/C	9.3	2.5-3.8	89.5 at 50 C	94 at 500 cycles at 50 C	26

Table S4. Full cell performance comparison

Symmetric full cell description	Voltage range [V]	Discharge capacity [mAh g^{-1}]	Cycle performance	Ref
NVP/NSC-75 ‖ 1M $NaPF_6$/Diglyme ‖ HC	**1.2-3.6**	**115.3 at 5 C**	**92.1%-5 C (800 cycles)**	**This work**
NMF-NVP/NC ‖ 1M $NaClO_4$/EC+DEC with FEC ‖ HC	1.5-3.7	75.9 at 5 C	60%-1 C (200 cycles)	27
NVP/C ‖ 1M $NaPF_6$/EC+DEC+FEC ‖ S-doped C	0.5-3.5	110 at 200 mA g^{-1}	90%-200 mA g^{-1} (100 cycles)	7
NVP@NSC ‖ 1M $NaClO_4$/EC+PC with FEC ‖ HC	2.0-3.8	98.5 at 100 mA g^{-1}	67.1%-1 C (100 cycles)	28
NVCP ‖ 1M $NaPF_6$/Diglyme ‖ HC	1.9-3.8	115.1 at 1 C	92.7%-1 C (150 cycles)	29
NVMP/C ‖ 1M $NaClO_4$ in EC/PC (1:1 v/v) ‖ HC	1.0-4.0	90 at 0.1 C	90%-1 C (100 cycles)	30
NVP-Na2.5% ‖ 1M NaClO4 in PC+FEC2%) ‖ HC	2.0-4.0	83.7 at 5 C	93.4%-5-0.5 C (100 cycles)	31
HP-NVP@SC ‖ 1M NaClO4 in EC/DMC (1:1 v/v) ‖ HP-NVP@SC	1.2-2.2	109.7 at 5 C	91.2%-5 C (1000 cycles)	9
NVP@rGO ‖ 1M $NaClO_4$ in EC/DEC (1:1 v/v) ‖ Sb/C	-	50 at 5 C	78%-0.5 C (40 cycles)	13
NVP: rGO-CNT ‖ 1M $NaClO_4$ in EC/DEC (1:1 v/v) ‖ NVP: rGO-CNT	1-2.2	110 at 1C	77%-10 C (100 cycles)	32
NVP/C-T ‖ 1M $NaPF_6$ in EC+DEC +FEC ‖ NVP/C-T	1.0-2.2	101.8 at 0.25 C	87%-2 C (200 cycles)	33

Reference

1. L. Li, Y. Li, Y. Ye, R. Guo, A. Wang, G. Zou, H. Hou and X. Ji, Kilogram-Scale Synthesis and Functionalization of Carbon Dots for Superior Electrochemical Potassium Storage, *Acs Nano*, 2021, **15**, 6872-6885.
2. J. Hafner, Ab-initio simulations of materials using VASP: Density-functional theory and beyond, *J. Comput. Chem.*, 2008, **29**, 2044-2078.
3. Blochl, Projector augmented-wave method, *Physical review. B, Condensed matter*, 1994, **50**, 17953-17979.
4. Perdew, Burke and Ernzerhof, Generalized Gradient Approximation Made Simple, *Phys. Rev. Lett.*, 1996, **77**, 3865-3868.
5. S. Grimme, Semiempirical GGA-type density functional constructed with a long-range dispersion correction, *J. Comput. Chem.*, 2006, **27**, 1787-1799.
6. X. Rui, X. Zhang, S. Xu, H. Tan, Y. Jiang, L. Y. Gan, Y. Feng, C. C. Li and Y. Yu, A Low-Temperature Sodium-Ion Full Battery: Superb Kinetics and Cycling Stability, *Adv. Funct. Mater.*, 2021, **31**, 2009458.
7. P. Feng, W. Wang, K. Wang, S. Cheng and K. Jiang, $Na_3V_2(PO_4)_{(3)}$/C synthesized by a facile solid-phase method assisted with agarose as a high-performance cathode for sodium-ion batteries, *J. Mater. Chem. A*, 2017, **5**, 10261-10268.
8. Y. Yao, Y. Jiang, H. Yang, X. Sun and Y. Yu, $Na_3V_2(PO_4)_{(3)}$ coated by N-doped carbon from ionic liquid as cathode materials for high rate and long-life Na-ion batteries, *Nanoscale*, 2017, **9**, 10880-10885.
9. W. Li, Z. J. Yao, Y. Zhong, C. A. Zhou, X. L. Wang, X. H. Xia, D. Xie, J. B. Wu, C. D. Gu and J. P. Tu, Enhancement of the advanced Na storage performance of $Na_3V_2(PO_4)_{(3)}$ in a symmetric sodium full cell via a dual strategy design, *J. Mater. Chem. A*, 2019, **7**, 10231-10238.
10. Y. Jiang, H. C. Zhang, H. Yang, Z. Y. Qi and Y. Yu, $Na_3V_2(PO_4)_{(3)}$@nitrogen, sulfur-codoped 3D porous carbon enabling ultra-long cycle life sodium-ion batteries, *Nanoscale*, 2017, **9**, 6048-6055.
11. W. Shen, H. Li, Z. Guo, C. Wang, Z. Li, Q. Xu, H. Liu, Y. Wang and Y. Xia, Double-Nanocarbon Synergistically Modified $Na_3V_2(PO_4)_{(3)}$: An Advanced Cathode for High-Rate and Long-Life Sodium-Ion Batteries, *ACS Appl. Mater. Interfaces*, 2016, **8**, 15341-15351.
12. C. Zhu, K. Song, P. A. van Aken, J. Maier and Y. Yu, Carbon-Coated $Na_3V_2(PO_4)_{(3)}$ Embedded in Porous Carbon Matrix: An Ultrafast Na-Storage Cathode with the Potential of Outperforming Li Cathodes, *Nano Lett.*, 2014, **14**, 2175-2180.
13. J. Zhang, Y. Fang, L. Xiao, J. Qian, Y. Cao, X. Ai and H. Yang, Graphene-Scaffolded $Na_3V_2(PO_4)_{(3)}$ Microsphere Cathode with High Rate Capability and Cycling Stability for Sodium Ion Batteries, *ACS Appl. Mater. Interfaces*, 2017, **9**, 7177-7184.
14. J. Yang, D.-W. Han, M. R. Jo, K. Song, Y.-I. Kim, S.-L. Chou, H.-K. Liu and Y.-M. Kang, $Na_3V_2(PO_4)_{(3)}$ particles partly embedded in carbon nanofibers with superb kinetics for ultra-high power sodium ion batteries, *J. Mater. Chem. A*, 2015, **3**, 1005-1009.
15. H. Xiong, G. Sun, Z. Liu, L. Zhang, L. Li, W. Zhang, F. Du and Z.-A. Qiao, Polymer Stabilized Droplet Templating towards Tunable Hierarchical Porosity in Single Crystalline $Na_3V_2(PO_4)_{(3)}$ for Enhanced Sodium-Ion Storage, *Angew. Chem. Int. Ed.*, 2021, **60**, 10334-10341.
16. Y. Huang, X. Lia, J. Wang, L. Miao, C. Li, J. Han and Y. Huang, Superior Na-ion storage achieved by Ti substitution in $Na_3V_2(PO_4)_{(3)}$, *Energy Storage Mater.*, 2018, **15**, 108-115.
17. J. Fang, S. Wang, Z. Li, H. Chen, L. Xia, L. Ding and H. Wang, Porous $Na_3V_2(PO_4)_3$@C

nanoparticles enwrapped in three-dimensional graphene for high performance sodium-ion batteries, *J. Mater. Chem. A*, 2016, **4**, 1180-1185.
18. E. Wang, W. Xiang, R. Rajagopalan, Z. Wu, J. Yang, M. Chen, B. Zhong, S. X. Dou, S. Chou, X. Guo and Y.-M. Kang, Construction of 3D pomegranate-like $Na_3V_2(PO_4)_{(3)}$/conducting carbon composites for high-power sodium-ion batteries, *J. Mater. Chem. A*, 2017, **5**, 9833-9841.
19. Y. Fang, L. Xiao, X. Ai, Y. Cao and H. Yang, Hierarchical Carbon Framework Wrapped $Na_3V_2(PO_4)_{(3)}$ as a Superior High-Rate and Extended Lifespan Cathode for Sodium-Ion Batteries, *Adv. Mater.*, 2015, **27**, 5895-5900.
20. J. F. Yang, D. D. Li, X. S. Wang, X. X. Zhang, J. Xu and J. T. Chen, Constructing micro-nano $Na_3V_2(PO_4)_{(3)}$/C architecture for practical high-loading electrode fabrication as superior-rate and ultralong-life sodium ion battery cathode, *Energy Storage Mater.*, 2020, **24**, 694-699.
21. Y. Jiang, Y. Yao, J. Shi, L. Zeng, L. Gu and Y. Yu, One-Dimensional $Na_3V_2(PO_4)_{(3)}$/C Nanowires as Cathode Materials for Long-Life and High Rate Na-Ion Batteries, *Chemnanomat*, 2016, **2**, 726-731.
22. L. Chen, Y. Zhao, S. Liu and L. Zhao, Hard Carbon Wrapped $Na_3V_2(PO_4)_{(3)}$@C Porous Composite Extending Cycling Lifespan for Sodium-Ion Batteries, *ACS Appl. Mater. Interfaces*, 2017, **9**, 44485-44493.
23. Q. Ni, Y. Bai, Y. Li, L. Ling, L. Li, G. Chen, Z. Wang, H. Ren, F. Wu and C. Wu, 3D Electronic Channels Wrapped Large-Sized $Na_3V_2(PO_4)_{(3)}$ as Flexible Electrode for Sodium-Ion Batteries, *Small*, 2018, **14**, 1702864.
24. S. Tao, X. Wang, P. Cui, Y. Wang, Y. A. Haleem, S. Wei, W. Huang, L. Song and W. Chu, Fabrication of graphene-encapsulated $Na_3V_2(PO_4)_{(3)}$ as high-performance cathode materials for sodium-ion batteries, *Rsc Advances*, 2016, **6**, 43591-43597.
25. B. Hou, L. Ma, X. Zang, N. Shang, J. Song, X. Zhao, C. Wang, J. Qi, J. Wang and R. Yu, Design and Construction of 3D Porous $Na_3V_2(PO_4)_{(3)}$/C as High Performance Cathode for Sodium Ion Batteries, *Chem. Res. Chin. Univ.*, 2021, **37**, 265-273.
26. S. Bao, Y. Y. Huang, S. H. Luo and J. L. Lu, Porous $Na_3V_2(PO_4)_{(3)}$/C as cathode material for high-rate sodium-ion batteries by sacrificed template method, *Ionics*, 2020, **26**, 5011-5018.
27. L. Zhao, H. Zhao, J. Wang, Y. Zhang, Z. Li, Z. Du, K. Swierczek and Y. Hou, Micro/Nano $Na_3V_2(PO_4)_{(3)}$/N-Doped Carbon Composites with a Hierarchical Porous Structure for High-Rate Pouch-Type Sodium-Ion Full-Cell Performance, *ACS Appl. Mater. Interfaces*, 2021, **13**, 8445-8454.
28. X. H. Liang, X. Ou, F. H. Zheng, Q. C. Pan, X. H. Xiong, R. Z. Hu, C. H. Yang and M. L. Liu, Surface Modification of $Na_3V_2(PO_4)_{(3)}$ by Nitrogen and Sulfur Dual-Doped Carbon Layer with Advanced Sodium Storage Property, *ACS Appl. Mater. Interfaces*, 2017, **9**, 13151-13162.
29. Y. Wang, G. Su, X. Li, L. Hou, L. Liang and C. Yuan, Boosting sodium-storage properties of hierarchical $Na_3V_2(PO_4)_{(3)}$@C micro-flower cathodes by tiny Cr doping: The effect of "four ounces moving a thousand pounds ", *Nano Research*, 2023, DOI: 10.1007/s12274-023-5555-8.
30. Y. B. Rao, K. R. Achary and L. N. Patro, Enhanced Electrochemical Performance of the $Na_3V_2(PO_4)_{(3)}$/C Cathode Material upon Doping with Mn/Fe for Na-Ion Batteries, *Acs Omega*, 2022, DOI: 10.1021/acsomega.2c06261.
31. X. Shen, Y. Su, N. Yang, X. Jiang, X. Liu, J. Mo, Y. Ran and F. Wu, Na plus -Activation Engineering in the $Na_3V_2(PO_4)_3$ Cathode with Boosting Kinetics for Fast-Charging Na-Ion Batteries, *ACS Appl. Mater. Interfaces*, 2022, DOI: 10.1021/acsami.2c12685.
32. C. Zhu, P. Kopold, P. A. van Aken, J. Maier and Y. Yu, High Power-High Energy Sodium Battery Based on Threefold Interpenetrating Network, *Adv. Mater.*, 2016, **28**,

2409-2416.
33. R. Ling, S. Cai, D. Xie, X. Li, M. Wang, Y. Lin, S. Jiang, K. Shen, K. Xiong and X. Sun, Three-dimensional hierarchical porous $Na_3V_2(PO_4)_{(3)}$/C structure with high rate capability and cycling stability for sodium-ion batteries, *Chem. Eng. J.*, 2018, **353**, 264-272.